Ab initio analytical Raman intensities for periodic systems through a coupled perturbed Hartree-Fock/Kohn-Sham method in an atomic orbital basis. II. Validation and comparison with experiments

Lorenzo Maschio, Bernard Kirtman, Michel Rérat, Roberto Orlando, and Roberto Dovesi

Citation: The Journal of Chemical Physics **139**, 164102 (2013); doi: 10.1063/1.4824443
View online: http://dx.doi.org/10.1063/1.4824443
View Table of Contents: http://scitation.aip.org/content/aip/journal/jcp/139/16?ver=pdfcov
Published by the AIP Publishing

Ab initio analytical Raman intensities for periodic systems through a coupled perturbed Hartree-Fock/Kohn-Sham method in an atomic orbital basis. II. Validation and comparison with experiments

Lorenzo Maschio,[1,a)] Bernard Kirtman,[2] Michel Rérat,[3] Roberto Orlando,[1] and Roberto Dovesi[1]

[1]*Dipartimento di Chimica, Università di Torino and NIS-Nanostructured Interfaces and Surfaces – Centre of Excellence, Via P. Giuria 7, 10125 Torino, Italy*
[2]*Department of Chemistry and Biochemistry, University of California, Santa Barbara, California 93106, USA*
[3]*Equipe de Chimie Physique, IPREM UMR5254, Université de Pau et des Pays de l'Adour, 64000 Pau, France*

(Received 16 August 2013; accepted 20 September 2013; published online 22 October 2013)

In this work, we validate a new, fully analytical method for calculating Raman intensities of periodic systems, developed and presented in Paper I [L. Maschio, B. Kirtman, M. Rérat, R. Orlando, and R. Dovesi, J. Chem. Phys. **139**, 164101 (2013)]. Our validation of this method and its implementation in the CRYSTAL code is done through several internal checks as well as comparison with experiment. The internal checks include consistency of results when increasing the number of periodic directions (from 0D to 1D, 2D, 3D), comparison with numerical differentiation, and a test of the sum rule for derivatives of the polarizability tensor. The choice of basis set as well as the Hamiltonian is also studied. Simulated Raman spectra of α-quartz and of the UiO-66 Metal-Organic Framework are compared with the experimental data. © *2013 AIP Publishing LLC*. [http://dx.doi.org/10.1063/1.4824443]

I. INTRODUCTION

In Paper I,[1] a new analytical LCAO-CO *ab initio* method for the evaluation of Raman intensities in crystalline (periodic) systems, at the Hartree-Fock (HF) and Density Functional Theory (DFT) level, was formulated. The nonresonant Raman susceptibilities were obtained, within the Placzek approximation,[2] using analytical partial derivatives of the polarizability tensor α with respect to atomic positions

$$\left.\frac{\partial \alpha_{b,c}}{\partial \mathcal{R}_a^A}\right|_{\mathcal{R}_0} = \left.\frac{\partial^3 E^{TOT}}{\partial \mathcal{R}_a^A \partial \mathcal{E}_b \partial \mathcal{E}_c}\right|_{\mathcal{E}=0,\mathcal{R}_0}. \quad (1)$$

Here, $\vec{\mathcal{R}}^A$ is the coordinate of atom A, $\vec{\mathcal{E}}$ is the electric field, and a, b, c indicate cartesian directions.

The purpose of the present paper is to validate this new implementation of the above formulation in the CRYSTAL code,[3,4] which uses a Gaussian Type Orbital (GTO) basis set, as well as to verify the methodology by comparison with numerical differentiation and with experiment.

Our method is not only much more efficient than treatments that require numerical differentiation, but also provides improved stability with respect to computational parameters, as will be demonstrated here. In addition, this general approach might in principle be extended to obtain other vibronic properties such as vibrational circular dichroism, sum frequency generation, hyper-Raman intensities, etc., without having to determine geometric wavefunction derivatives or carry out numerical differentiation with respect to the wavevector.

There exist only a few previous methods for the simulation of Raman spectra in crystalline materials. All of them have reached maturity recently[5–10] and all have been developed within the framework of a plane wave basis. The main application of such methods has been in the study of minerals.[11–14] To our knowledge, the formulation presented in Paper I[1] and tested here is the first analytical treatment of Raman intensities suitable for GTO basis sets.

In Sec. II, we begin by establishing the stability of the calculations with respect to the computational parameters. Then, two model systems are used to test the dimensional consistency in going from 0D (molecules) to 1D (polymers) to 2D (slabs) and, finally, to 3D (bulk) systems. This strategy was previously adopted to validate the implementation of the Coupled-Perturbed Hartree-Fock/Kohn Sham (CPHF/KS) method[15] for electronic hyperpolarizabilities and infrared intensities[16] in CRYSTAL. 0D results can be compared with those produced by molecular codes; the smooth convergence from finite to infinite directions, especially when passing from 2D to 3D, confirms the high stability of the algorithms. As a more direct internal test, this is followed by a comparison with numerical differentiation and, finally, the translational sum rule is checked.

Section III deals with experimental comparisons; for the purposes of this paper, we have chosen to study two very different cases.

The first case is a relatively simple system, the α polymorph of crystalline quartz. α-SiO_2 has long been a favourite benchmark for the simulation of Raman spectra.[5,8,10] It commonly exists in a rather pure crystalline phase, which is why it is widely used as the reference for tuning of instruments. Indeed, most recent advances in experimental techniques rely

a)Electronic mail: lorenzo.maschio@unito.it.

TABLE I. Effect of integral screening threshold T (see text) on computed Raman intensities for the 12 Raman-active normal modes of α-quartz. Mean Absolute Error (MAE) and Mean Absolute Relative Error (MARE) are reported, with T = 20 taken as the reference. A label (mode #) is assigned to each mode (some are degenerate) to be used in other tables. Values in bohr^4/amu.

Mode #	1	2	3	4	5	6	7	8	9	10	11	12			
freq. (cm^{-1})	149	231	292	385	437	506	516	745	848	1130	1144	1240	MAE	MARE	$\|\Delta\|_{max}$
T															
6	394.57	1174.25	168.00	406.09	362.87	881.92	6044.84	158.90	782.10	226.49	152.97	1057.84	14.89	2.17%	74.00
8	397.53	1151.19	164.42	401.63	369.23	885.16	6020.72	150.67	762.77	221.04	141.81	1098.77	11.41	0.91%	98.12
10	398.65	1173.70	166.91	399.72	371.31	884.39	6103.48	152.45	763.16	223.39	144.85	1094.89	2.71	0.45%	15.36
12	399.53	1167.83	165.91	398.88	373.72	886.09	6130.80	152.20	765.65	225.79	142.80	1100.36	2.25	0.32%	11.96
14	398.45	1167.82	165.94	400.13	374.16	884.96	6120.61	151.51	764.93	226.40	143.39	1100.03	0.94	0.16%	2.92
16	398.12	1168.69	165.97	399.76	373.63	884.66	6114.73	151.27	764.20	226.70	143.38	1098.02	0.78	0.12%	4.11
18	397.93	1170.01	166.20	399.84	373.67	884.69	6117.56	151.05	764.40	226.98	143.24	1098.11	0.43	0.11%	1.28
20	397.92	1170.74	166.11	399.89	373.36	884.51	6118.84	151.52	763.72	227.60	143.72	1098.38			

on this system.[17] While providing a further check on the method and implementation, the major purpose of the comparison made here is to assess the effect of basis set and energy functional on the computed intensities.

The second case is a considerably more complex Metal-Organic Framework (MOF) structure. MOFs are amongst the most promising new materials for a variety of applications.[18] In fact, they are already used for gas storage, gas separation, catalysis, and sensors. The structure of MOFs is characterized by metal ions or clusters coordinated with organic molecules to form stable microporous three-dimensional materials. Raman spectroscopy is an important tool for the study of such systems, since it is capable of detecting changes due to defects, presence of solvent, or interaction with gas molecules. In Sec. III C, we report the B3LYP simulated spectrum of UiO-66,[19] one of the most interesting, recently discovered, MOFs. It is a fairly complex system with 114 atoms in the unit cell and 90 Raman-active vibrational modes (considering degenerate modes only once).

II. INTERNAL VALIDATION OF METHOD AND IMPLEMENTATION IN THE CRYSTAL CODE

In this section, we assess the correctness of the formulation given in Paper I[1] as well as the implementation in CRYSTAL through inner checks. After testing the effect of computational thresholds (Sec. II A), two validation schemes have been used: (i) consistency through model systems of increasing dimensionality – Sec. II B, and (ii) more directly by comparing the analytical scheme with numerical derivatives of the dielectric tensor with respect to Cartesian coordinates of atoms in the unit cell – Sec. II C. Finally, in Sec. II D we check that the computed intensities satisfy the sum rule.[9]

A. Stability with respect to computational parameters

Before carrying out the internal checks, it is necessary to investigate the computational parameters. Amongst the several parameters involved in the calculation, we have determined that default values for the thresholds regulating SCF convergence,[3] first- and second-order CPHF convergence (CPHF1 and CPHF2),[15,20,21] and the determination of analytical gradients[22] are sufficient for our purposes.[23]

As discovered previously in the case of IR intensities,[16] the only parameters in the CRYSTAL program that have an appreciable effect on the Raman intensities are the integral screening thresholds. There are five such parameters in CRYSTAL;[24,25] 10^{-T_1} and 10^{-T_3} are overlap thresholds for Coulomb and Exchange integrals, 10^{-T_2} is the penetration threshold for Coulomb integrals, while 10^{-T_4} and 10^{-T_5} are pseudo-overlap thresholds for the truncation of HF exchange series. For further details on these parameters, the reader can refer to the CRYSTAL manual.[3] We reduce these five thresholds to one by taking $T_1 = T_2 = T_3 = T_4 = T$, $T_5 = 2T$; the default value is $T = 6$. We tested the effect of varying T using the α-quartz crystal[26] with the results reported in Table I for all Raman active modes (see Eq. (5) below for intensity formula). It may be seen that the mean absolute relative error (MARE) with respect to the most accurate results ($T = 20$), is about 2% for the default value ($T = 6$). It decreases to less than 1% and 0.5% at $T = 8$ and $T = 10$, respectively, and becomes insignificant at $T \geq 14$. The maximum absolute error $|\Delta|_{max}$ is associated with the most intense (516 cm^{-1}) mode for all T values except T = 14, in which case it corresponds to the second most intense mode (231 cm^{-1}). We single out $T = 10$ as a good compromise between high accuracy and computational cost, to be used in remaining calculations of Sec. II for numerical validation. Lower values $T = 6$ or 8 can be regarded as more than satisfactory for all practical purposes, i.e., comparison with experiments.

B. From the molecule to the bulk: Comparison of periodic and nonperiodic treatments

Now we are ready to consider the evolution of the Raman intensities with increasing dimensionality. For this purpose, two model systems differing with regard to atomic species, structural properties, and type of chemical bonding were considered:

- n-dimensional LiF structures were built by assembling a finite number of (n−1)-dimensional structures progressively. Accordingly, we connected LiF molecules (0D LiF) to form linear chains of different lengths,

TABLE II. Comparison of polarizability tensor derivatives obtained from finite system calculations with infinite periodic results for distorted LiF structure and hexagonal BN. N denotes the number of molecules used to form a finite linear chain (along x) or the number of chains forming a finite monolayer (along y) or the finite thickness of a slab (along z). Unit cell geometrical parameters are fixed at bulk values and the lattice parameters are given in the text. The screening thresholds (see text) are set to T = 10. The entry with an asterisk corresponds to the value corrected for the difference between the microscopic and macroscopic electric field according to Eqs. (2) and (3). Only those elements (boldfaced) corresponding to polarizability components with at least one z index require correction. All derivatives are given in bohr^2.

		LiF					Hexagonal BN
	N	$\partial\alpha_{xx}/\partial\mathcal{R}_x^{Li}$	$\partial\alpha_{yy}/\partial\mathcal{R}_x^{Li}$	$\partial\alpha_{zz}/\partial\mathcal{R}_x^{Li}$	$\partial\alpha_{xy}/\partial\mathcal{R}_y^{Li}$	$\partial\alpha_{xz}/\partial\mathcal{R}_z^{Li}$	$\partial\alpha_{xx}/\partial\mathcal{R}_x^{B}$
Molecule	1	− 0.9568	− 0.0588	− 0.0588	− 0.1333	− 0.1333	
	3	− 0.7733	0.0022	0.0022	0.0048	0.0048	
	7	− 0.7408	− 0.0041	− 0.0041	0.0124	0.0124	
	15	− 0.7384	− 0.0054	− 0.0054	0.0134	0.0134	
	35	− 0.7374	− 0.0056	− 0.0056	0.0135	0.0135	
	50	− 0.7372	− 0.0056	− 0.0056	0.0135	0.0135	
	75	− 0.7372	− 0.0057	− 0.0057	0.0136	0.0136	
Chain	1	− 0.7372	− 0.0057	− 0.0057	0.0136	0.0136	
	3	− 0.5060	− 0.0301	− 0.0313	0.0073	0.0171	
	7	− 0.5364	− 0.0518	− 0.0210	0.0160	0.0181	
	15	− 0.5367	− 0.0546	− 0.0202	0.0157	0.0175	
	35	− 0.5367	− 0.0564	− 0.0198	0.0156	0.0171	
	50	− 0.5367	− 0.0568	− 0.0197	0.0156	0.0170	
	100	− 0.5365	− 0.0572	− 0.0197	0.0156	0.0170	
	150	− 0.5365	− 0.0574	− 0.0196	0.0156	0.0169	
Slab	1	− 0.5365	− 0.0577	− 0.0196	0.0156	0.0168	− 12.2356
	3	− 0.3927	0.0081	0.0057	0.0329	0.0061	− 10.8123
	5	− 0.3995	− 0.0011	− 0.0004	0.0346	0.0113	− 10.7895
	7	− 0.3999	− 0.0011	− 0.0004	0.0348	0.0133	− 10.7927
	9	− 0.4003	− 0.0011	− 0.0004	0.0346	0.0137	
	11	− 0.4004	− 0.0010	− 0.0004	0.0346	0.0137	⋮
	13	− 0.4004	− 0.0010	− 0.0004	0.0345	0.0137	
	*13	− 0.4004	− 0.0010	**− 0.0010**	0.0345	**0.0345**	− 10.7927
Bulk	...	− 0.4004	− 0.0010	− 0.0010	0.0345	0.0345	− 10.7927

ideally evolving to an infinite linear chain (1D LiF). In turn, infinite linear chains were arranged next to each other in a plane by alternating Li and F ions along the growing direction to form an infinite LiF layer (2D LiF). Finally, we superimposed infinite LiF layers to form slabs of growing thickness to eventually approximate bulk LiF (3D LiF). In all cases, one of the Li atoms is at the origin of the unit cell and the lattice constant is that of bulk 3D LiF, i.e., 4.017 Å.

The bulk crystal is cubic, with space group $Fm\bar{3}m$. If the Li–F distances are kept at $a/2$ (symmetric case, with equivalent Li–F and F–Li distances), there are no Raman-active vibrations by symmetry. Thus, the F ion at (0.5, 0.0, 0.0) was shifted to 0.45 along the x direction.

All calculations were performed at the Hartree-Fock level with a basis set consisting of a 6-1 contraction (one *s* and one *sp* shell) for Li, and a 7-311(1) contraction for F (one *s*, three *sp*, and one *d* shell). The exponents of the most diffuse shells were $\alpha_{Li}^{sp} = 0.525$, $\alpha_F^{sp} = 0.437$ and 0.137, and $\alpha_F^d = 0.6$ bohr^{-2}.

- Two-dimensional graphene-like sheets of hexagonal boron nitride (BN) were stacked to simulate the bulk crystalline structure for comparison with a direct 3D calculation. The basis set was 6-21G* on both B and N and the lattice parameters were set to the experimental geometry ($a = 2.501$ Å and $c = 6.66$ Å),[27] with a hexagonal 3D unit cell belonging to the $P6_3/mmc$ space group. Again, the calculations were performed at the Hartree-Fock level.

Both model systems have two atoms in the unit cell so that, in the 3D limit, the Raman tensor elements will be equal for each atom, but opposite in sign (according to the sum rule, *vide infra*). It is, then, sufficient to look at one atom (we chose Li for LiF, B for BN). In each case, the values in Table II refer to the unit cell at the center of the system, i.e., the central molecule in the linear chain, the central polymer in the planar arrangement, and so on.

Let us consider first the LiF results; x is the linear chain direction and the slab lies in the xy plane. Starting from the isolated molecule, we see that convergence to the infinite periodic chain limit (see N = 1 in chain block) is rapidly achieved. At N = 15, the difference between the two for all five components is within about 0.0015 bohr^2. Nevertheless, a very long chain (N = 75) is needed to reach full convergence within the

reported four decimal figures. At this large N limit, the finite chain results coincide perfectly with the values obtained for the infinite periodic polymer. This provides evidence that the present periodic implementation is correct and that the numerical accuracy is very high. The evolution from 1D polymer to 2D periodic slab is also smooth, although in this case the convergence is much slower for $\partial\alpha_{yy}/\partial\mathcal{R}_x^{Li}$. At N = 150, the error is still about 0.0003 bohr^2.

The convergence of stacked planes to the bulk system is much faster, as previously observed for polarizabilities[20] and Born charges.[16] In fact, 9 layers are sufficient to reach the limiting infinite periodic value within 0.0001 bohr^2. Note that, in order to compare the stacked layers with the bulk, derivatives involving the z direction of the polarizability tensor must be corrected to account for the difference between the microscopic and macroscopic electrostatic fields (see Table I and related text of Ref. 15). For α_{zz},

$$\frac{\partial\alpha_{zz}^{3D}}{\partial\mathcal{R}_x^A} = \epsilon_{zz}^2 \frac{\partial\alpha_{zz}^{2D}}{\partial\mathcal{R}_x^A} \tag{2}$$

whereas the expression for mixed directions, like xz, is slightly more complicated

$$\frac{\partial\alpha_{xz}^{3D}}{\partial\mathcal{R}_z^A} = \epsilon_{zz} \frac{\partial\alpha_{xz}^{2D}}{\partial\mathcal{R}_z^A} + 2\chi_{xzz}^{(2)} Z_{zzA}^{*2D} \ . \tag{3}$$

In these equations, ϵ_{zz} is the zz component of the bulk dielectric tensor, $\chi_{xzz}^{(2)}$ is the xzz component of the bulk first nonlinear electric susceptibility, and $Z_{zzA}^{*2D} = \partial^2 E^{TOT}/\partial\mathcal{R}_z^A\partial\mathcal{E}_z$ is the zz component of the Born charges tensor (cf. Eq. (1) of Ref. 16). More details on the derivation of these expressions are given in the Appendix.

For LiF, the value of ϵ_{zz}, computed by the CPHF method,[15,20] is 1.6631, while χ_{xzz} and Z_{zzLi}^{*2D} are 0.0092 and 0.6295, respectively (in atomic units).

The results obtained for hexagonal boron nitride (last column of Table II) entirely confirm the above conclusions. In this case, only the 2D → 3D convergence can be checked, which is achieved very rapidly (seven layers are sufficient).

C. Comparison with numerical derivatives

In order to further validate our method, we have compared analytical CPHF results to those obtained by numerical differentiation of the polarizability tensor using finite atomic displacements. To achieve good accuracy with the latter method, a three-point (0.000 ± 0.003 a.u.) formula has been used.

In Table III, the transverse optical (TO) modes of powder α-quartz (SiO_2) and calcite ($CaCO_3$) are reported as computed by the two schemes. For calcite, the basis set is the same as in Ref. 28, while for α-SiO_2 the basis set is the one described earlier in this paper. The excellent agreement between the two methods constitutes, in our opinion, a strong validation of our fully analytical scheme. The same agreement was observed for CPKS results that we do not report here.

In the analytical method, the computational cost for obtaining the complete set of Raman intensities is essentially that of three CPHF cycles for the $U^{(\mathcal{E}_b)}(\vec{k})$ perturbation matrices (one for each direction) and six CPHF2 cycles for $U^{(\mathcal{E}_b,\mathcal{E}_c)}(\vec{k})$ (see Sec. II B of Paper I[1]). The cost is roughly the same for each cycle. In the case of numerical differentiation using the three-point formula, $2 \times 3\mathcal{N}$ CPHF cycles are needed for each polarizability component, with $\mathcal{N}$ being the number of irreducible atoms in the unit cell (each atom in the cell is moved along x, y, and z). Even though $\mathcal{N}$ is small for the cases considered here, the speedup factor is nearly 10 as shown in the caption of Table III. Here, the wall clock timing refers to the calculation of the Raman intensities only; the time needed for frequencies is not included.

TABLE III. Comparison of numerical finite difference with analytical Raman absolute intensities for the active TO modes of calcite and α-quartz. The wall clock timings, referring to a parallel run on 64 cores (2.70 GHz Xeon), are 1.5 h (analytical) vs. 14.6 h (numerical) for $CaCO_3$ and 1.0 h vs. 7.9 h for SiO_2.

	Frequency ν (cm^{-1})	Intensity (bohr^4 amu^{-1}) num.	Intensity (bohr^4 amu^{-1}) anal.	Abs. difference (%)
$CaCO_3$	155	1800.8	1792.7	0.5
	277	12 192	12 234	0.3
	711	12 101	12 065	0.3
	1089	68 241	68 341	0.1
	1434	9319.7	9280.7	0.4
SiO_2	149	397.94	398.65	0.1
	231	1174.6	1173.7	0.1
	292	165.86	166.91	0.6
	385	399.30	399.72	0.1
	437	372.61	371.31	0.3
	506	884.35	884.39	0.0
	516	6104.7	6103.4	0.0
	745	151.33	152.45	0.7
	848	761.53	763.16	0.2
	1130	224.93	223.39	0.7
	1144	143.09	144.85	1.2
	1240	1094.1	1094.8	0.0

Note that the analytical scheme does not depend upon additional parameters (step size, number of points) that must be defined and checked in the numerical scheme to ensure accuracy.

D. Sum rule

The derivative of each component of the Raman tensor in the three Cartesian directions must obey the acoustic sum rule

$$\sum_A \frac{\partial\alpha_{bc}}{\partial\mathcal{R}_a^A} = 0, \tag{4}$$

where the sum is over all atoms in the unit cell. This follows from the consideration that polarizabilities must be invariant under global translation of the whole crystal; this is formally satisfied by Eq. (77) of Paper I[1] since all involved matrices are translationally invariant by construction. This rule can be taken as a measure of the numerical precision of the implemented method. In fact, its value has been used in literature to derive a rule of thumb for correction of the computed intensities.[9] In other cases, discrepancies of about 2% were attributed to "numerical noise."[7] In *all* our test calculations

(including those reported in Secs. III A–III C), this rule was satisfied at least up to 10^{-10} bohr^2.

III. COMPARISONS WITH EXPERIMENT

When simulating the experimental Raman spectrum of a real crystal, a number of factors must be taken into account. The relevant formulas, which are well-known, are briefly summarized here for ease of reference. For an oriented single-crystal, the Raman Stokes scattering intensity associated with, for instance, the *xy* component of the polarizability tensor corresponding to the *i*-vibrational mode of frequency ω_i may be calculated as

$$I^i_{xy} \propto C \left(\frac{\alpha_{xy}}{\partial \mathcal{Q}_i} \right)^2, \tag{5}$$

where $\mathcal{Q}_i$ is the the normal mode coordinate for mode *i*. The prefactor C depends[9,29] on the laser frequency ω_L and the temperature T

$$C \sim (\omega_L - \omega_i)^4 \frac{1 + n(\omega_i)}{30\omega_i} \tag{6}$$

with the Bose occupancy factor $n(\omega_i)$ given by

$$1 + n(\omega_i) = \left[1 - \exp\left(-\frac{\hbar\omega_i}{K_B T} \right) \right]^{-1}. \tag{7}$$

The polycrystalline (powder) spectrum can be computed by averaging over the possible orientations of the crystallites as described in Eqs. (4) and (5) of Ref. 11, which we used for our implementation.

While the intensity of the TO modes is straightforwardly computed once the appropriate polarizability derivative is obtained, the corresponding calculation for longitudinal optical (LO) modes requires a correction[9,30] due to $\chi^{(2)}_{bcd}$

$$\left. \frac{\partial \alpha_{b,c}}{\partial \mathcal{R}^A_a} \right|_{\mathcal{R}_0} = \frac{1}{V} \left. \frac{\partial^3 E^{TOT}}{\partial \mathcal{R}^A_a \partial \mathcal{E}_b \partial \mathcal{E}_c} \right|_{\mathcal{E}=0,\mathcal{R}_0} - 2 \sum_{b'} Z^*_{b'aA} \sum_{d'} \epsilon^{-1}_{b',d'} \chi^{(2)}_{bcd'}. \tag{8}$$

In Eq. (8), ϵ^{-1} is the inverse of the high-frequency (i.e., pure electronic) dielectric tensor. $\chi^{(2)}$ is defined as in Eq. (69) of Ref. 15. Finally, as commonly done in the reporting of experimental data, the intensities are normalized here to the highest peak, arbitrarily set to 1000.00.

A. Basis set and functional dependency

Six different SiO_2 basis sets were used for investigating the basis set effect. They can be grouped into three "families":

(a) Two sets were taken from the CRYSTAL database:[31] a first set with 66-21G* contractions on Si and 6-31G* on O, and a second with 86-311G** on Si[32] and 8-411d11 on O.[33] We will refer to these basis sets as "a1" and "a2."
(b) The Peintinger–Oliveira–Bredow (pob) basis sets denoted as pob-TZVP and pob-TZVPP.[34]
(c) Two sets from an earlier study of the vibrational properties of α-quartz using the CRYSTAL code,[35] and previously labeled as "2*d*" and "2*d* + *f*." These are actually modifications of a Pople 6-21G* basis (on Si) and 6-31G* (on O), where one *d*-type function has been added to each atom in the first case and, in the second case, an *f*-type function as well.

TABLE IV. Normalized Raman intensities for TO modes of α-SiO_2 computed with different basis sets (see text) at the B3LYP level.

Basis set	a1	a2	pob-TZVP	pob-TZVPP	2*d*	2*d* + *f*
Mode #						
1	45.74	42.06	24.22	24.71	25.72	28.17
2	184.16	212.77	185.11	177.17	196.63	208.44
3	18.35	18.27	12.22	13.08	13.69	15.47
4	55.99	43.53	27.41	31.86	40.31	36.77
5	45.50	37.94	21.79	23.14	39.04	37.55
6	100.55	63.25	26.61	27.13	28.68	31.81
7	1000.00	1000.00	1000.00	1000.00	1000.00	1000.00
8	49.94	27.78	26.39	25.04	44.45	43.08
9	109.62	53.94	40.41	44.07	74.51	70.55
10	27.32	28.26	34.94	40.56	46.94	43.56
11	22.04	22.42	25.36	28.27	34.22	31.72
12	135.87	90.43	82.40	95.25	143.29	128.79

We do not enter here into a discussion about the sensitivity of the vibrational modes to basis set and hamiltonian. Suffice it to say that there are several modes in α-SiO_2 that depend strongly on the soft Si–$\widehat{O}$–Si angle which, in turn, appears to be very sensitive to the adopted basis set.[35,36] For that reason, we have carried out our investigation at fixed lattice geometry (re-optimizing the internal coordinates for each basis set and hamiltonian). Our results for the computed intensities are reported in Table IV. In spite of the variation in relative intensities, the order of the most intense modes is reproduced by all basis sets, that is, $I^7 > I^2 > I^{12}$ (for all basis sets but a2, $I^{12} > I^9$ as well), where I^m indicates the intensity of the *m*th mode (cf. Table I). In Table V, we reported the MARE and MAE (mean absolute error) in a cross-comparison between all the basis sets. These results show that the a1 basis (the lowest quality) clearly differs from the others (by up to 90% MARE) and must be considered too poor. As regard the others, the MARE ranges up to 44%, and the MAE is as large as 18, indicating that the computed intensities must be taken with some caution. It should be mentioned that a similar uncertainty affects the measured intensities, because of experimental difficulties in obtaining reliable relative intensities across the entire frequency range.[37] As a consequence of such fluctuations in the computed and measured intensities, comparisons of the two can be made only on a semi-quantitative basis.

In Table VI, Raman intensities of α-SiO_2 computed using different Hamiltonians and the $2d + f$ basis are reported. Again, only fractional coordinates were optimized in each calculation. The impact of the Hamiltonian is overall much smaller than the basis set effect, in spite of the fact that a broad range of functionals (LDA, GGA, hybrid) is covered. The discrepancy is more relevant for HF results, but in all

TABLE V. Cross-comparison of mean absolute relative error (MARE, %) and mean absolute error (MAE; units corresponding to normalized intensities) relative to the data of Table IV.

		a2	pob-TZVP	pob-TZVPP	2*d*	2*d* + *f*
MARE	a1	33.5%	90.1%	83.4%	51.3%	47.9%
	a2	...	44.4%	41.2%	37.7%	31.0%
	pob-TZVP		...	7.8%	25.9%	26.1%
	pob-TZVPP			...	21.2%	21.1%
	2*d*				...	7.8%
MAE	a1	19.5	28.4	27.6	18.9	20.0
	a2	...	13.9	14.2	18.1	14.0
	pob-TZVP		...	3.8	16.1	15.4
	pob-TZVPP			...	13.2	14.0
	2*d*				...	4.8

cases the larger intensities remain in the order $I^7 > I^2 > I^{12} > I^9$. The relative insensitivity to the chosen Hamiltonian parallels the experience in molecular simulations, where no appreciable change in intensities is observed on representative sets of molecules, even when *ab initio* correlated methods (MP2) are included in the comparison.[38,39]

B. The α-quartz crystal

The simulated Raman powder spectrum of α-quartz is reported in Fig. 1 along with the experimental one.[40] Both TO and LO modes are included. Data refer to 300 K, with an incoming laser frequency of 514.5 nm. Corrections for the laser frequency and temperature, as well as averaging over orientations for the polycrystalline sample, were carried out as described at the beginning of this section. A Lorentzian broadening of 5 cm^{-1} was adopted. Low intensities have been amplified 10 times and reported as a thin line. Both the theoretical and experimental spectra are normalized to the highest peak. We have used the B3LYP functional and the pob-TVZP basis.

The figure shows that the experimental spectrum is reproduced remarkably well, especially in the high frequency region (i.e., above 600 cm^{-1}). A slight overestimation of the intensity of modes at about 700 and 1200 cm^{-1} is observed, while other parts of the profile are faithfully reproduced. The double peak at 800 cm^{-1} is due to the LO-TO splitting (left peak is TO, right is LO).

In the low frequency region of the spectrum, the agreement is somewhat less good. Our treatment does not give the peak width and, as just mentioned, the Lorentzian spread we use is fixed, while the bands immediately below and above 200 cm^{-1} exhibit a significant variation in this respect. A slight overestimation of the computed intensities in this frequency region can be observed. Since we do not have access to the experimental details, these aspects will not be discussed any further.

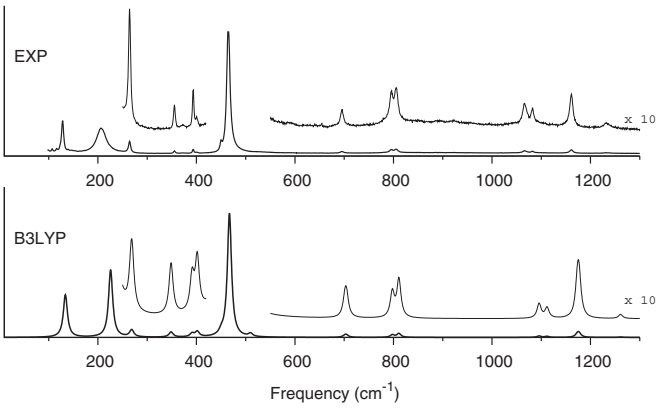

FIG. 1. Computed (B3LYP, pob-TZVP basis set) and experimental Raman spectrum of α-SiO_2. Both LO and TO modes are included in the computed spectra. Curves are normalized to the highest peak and reported in arbitrary units. The low intensity peaks are also shown magnified by a factor of ten. For further details, see Sec. III B.

TABLE VI. Raman intensities of α-SiO_2 TO modes obtained using the 2*d* + *f* basis set (see text) and different Hamiltonians.

Hamiltonian	HF	LDA	PBE	B3LYP
Mode #				
1	35.06	23.99	22.16	28.17
2	211.52	195.98	192.80	208.44
3	18.71	13.25	12.03	15.47
4	33.58	39.30	34.02	36.77
5	46.70	33.33	29.30	37.55
6	43.66	19.53	24.10	31.81
7	1000.00	1000.00	1000.00	1000.00
8	23.06	52.68	55.59	43.08
9	73.65	66.87	72.46	70.55
10	67.54	36.88	37.03	43.56
11	38.97	26.09	29.15	31.72
12	173.88	121.40	111.06	128.79

C. UiO-66 metal-organic framework

UiO-66 is a recently discovered[19,41] microporous material whose structure is based on a $Zr_6O_4(OH)_4$ octahedron, with lattices formed by 12-fold connection through a 1,4-benzene-dicarboxylate (BDC) linker. A full characterization of the structure and vibrational modes has been possible through a synergy between experiment and *ab initio* calculation, as reported by Valenzano *et al.*[42] We refer to that work for the crystal structure and computational parameters adopted;[43] the vibrational modes can be visualized on the CRYSTAL website.[44] Our main focus here is on Raman intensities.

Our calculation uses 1580 atomic orbitals centered on the 114 atoms in the unit cell. There are 90 Raman active modes (each degenerate mode is counted once). The simulated and experimental spectra are shown in Figure 2 with the experimental spectrum being the same as in panel (g′) of Figure 3 of Ref. 45. We note that the latter spectrum was recorded in air, which might cause small differences with respect to our calculations.

The agreement on the intensity of the main peaks is very good, with some underestimation of the experimental relative intensities for the modes around 1150 and 850 cm^{-1}.

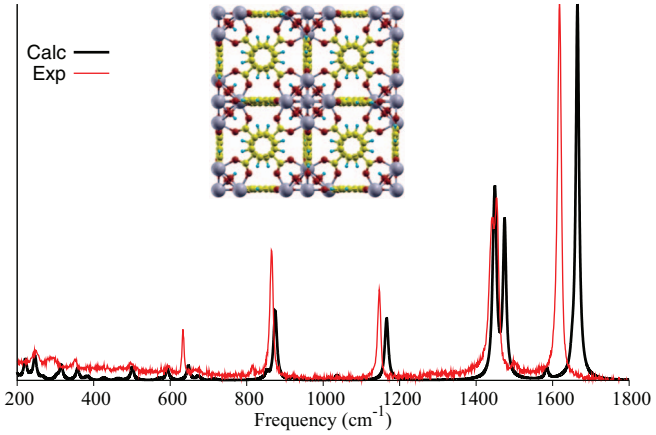

FIG. 2. Experimental[45] and calculated Raman spectrum of hydroxylated UiO-66 Metal-Organic Framework. The unit cell is also shown in the figure.

The vibrational modes of UiO-66 that lie above 800 cm^{-1} are those involving the organic ligands, which vibrate freely in the framework cages, much like a gas phase molecule. The low frequency region, which is less well-defined experimentally, is dominated by modes that involve the Zr atom. Despite the shifting baseline, however, several experimental peaks can be recognized.

In Figure 3, we report the deconvolution of Raman peaks in the region 1350–1800 cm^{-1}. The high frequency peak at 1664 cm^{-1} is actually a combination of one A_g, two E_g, and three F_{2g} modes, with comparable intensities. These modes all correspond to in-phase (A_g) or out of phase (E_g, F_{2g}) vibrations of the organic linker as noted above. All of these modes contribute to the intensity of the 1664 cm^{-1} peak, with the E_g modes having a lesser role. This means that the 12 linkers are distant enough, in the unit cell, to make their interaction negligible. Such an analysis could be important to understand the nature of vibrations in these soft materials.

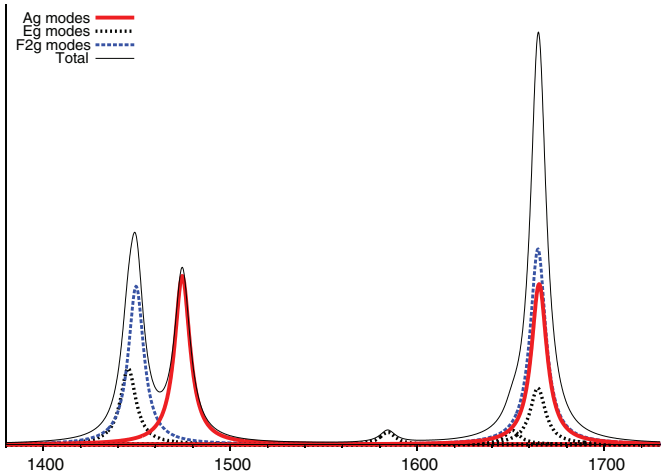

FIG. 3. Deconvolution of Raman peaks in the region 1350-1800 cm^{-1} of the UiO-66 spectrum (cf. Fig. 2).

IV. CONCLUSIONS

Our method for the efficient analytical calculation of Raman intensities presented in Paper I[1] has been validated through internal tests and comparison with the experiment. After establishing the stability with respect to integral screening tolerances, we demonstrated: (i) the consistency for increasing number of periodic directions (0D → 1D → 2D → 3D), (ii) the accuracy as compared to numerical differentiation, and (iii) the fact that the sum rule for individual tensor components is always very well satisfied. From tests on alpha-quartz, it was established that the computed intensities are relatively insensitive to the choice of DFT functional but do depend substantially on the basis set.

Raman spectra calculated for α-SiO_2 and UiO-66 MOF with the B3LYP functional were found to agree very well with experiment. This includes not only the main peaks but also smaller features. The UiO-66 crystal, in particular, provides a fairly challenging computational task since there are more than a hundred atoms in the unit cell.

Further work in the development and application of the computational tool presented here and in Ref. 1 is envisioned. We want to examine more accurate experimental data, possibly measured at low temperature and with such equipment to guarantee better consistency of the collected data throughout the entire spectrum. In addition, experiments using polarized light on single crystals will also be of interest.

ACKNOWLEDGMENTS

L.M. thanks Francesca Bonino for providing the original data of the experimental UiO-66 Raman spectrum.

APPENDIX: FROM 2D TO 3D FOR LIF

Let z be the direction perpendicular to a 2D slab. We define α_{zz}^{3D} as the zz-component of the polarizability of a unit cell in the bulk, and α_{zz}^{2D} as the corresponding quantity for the slab obtained as the average over all layers. In the bulk, the field felt by the atoms of the unit cell is the macroscopic field $\mathcal{E}_z$, which includes the polarization of the crystal, while for the slab it is the microscopic (or displacement) field $\mathcal{E}_{0z} = \epsilon_{zz}\mathcal{E}_z$. Then, we have: $\alpha_{zz}^{3D} = d\mu_z/d\mathcal{E}_z = \epsilon_{zz}(d\mu_z/d\mathcal{E}_{0z}) = \epsilon_{zz}\alpha_{zz}^{2D}$, while $\alpha_{xx}^{3D} = \alpha_{xx}^{2D}$. Thus,

$$\frac{d\alpha_{zz}^{3D}}{d\mathcal{R}_x^A} = \frac{\partial\alpha_{zz}^{3D}}{\partial\mathcal{R}_x^A} + \frac{\partial\alpha_{zz}^{3D}}{\partial\mathcal{E}_z}\frac{\partial\mathcal{E}_z}{\partial\mathcal{R}_x^A} = \frac{\partial\alpha_{zz}^{3D}}{\partial\mathcal{R}_x^A}. \tag{A1}$$

The second term in first equality arises because the polarization vector is non-zero in the z-direction.[30] However, this term vanishes because the hyperpolarizability component $\beta_{zzz}^{3D} = \partial\alpha_{zz}^{3D}/\partial\mathcal{E}_z$ is equal to zero for cubic LiF. This leads to

$$\frac{d\alpha_{zz}^{3D}}{d\mathcal{R}_x^A} = \epsilon_{zz}\frac{\partial\alpha_{zz}^{2D}}{\partial\mathcal{R}_x^A} + \alpha_{zz}^{2D}\frac{\partial\epsilon_{zz}}{\partial\mathcal{R}_x^A}. \tag{A2}$$

Using the fact that the depolarization factor is 4π in the z-direction: $\epsilon_{zz} = 1 + 4\pi\alpha_{zz}^{3D}/V$ (V is the volume of the unit

cell, which is held constant here), Eq. (A2) becomes

$$\frac{\partial \alpha_{zz}^{3D}}{\partial \mathcal{R}_x^A} = \epsilon_{zz} \frac{\partial \alpha_{zz}^{2D}}{\partial \mathcal{R}_x^A} + \frac{4\pi \alpha_{zz}^{2D}}{V} \frac{\partial \alpha_{zz}^{3D}}{\partial \mathcal{R}_x^A}. \tag{A3}$$

From the relationship between α_{zz}^{3D} and α_{zz}^{2D}, we may also write: $\epsilon_{zz} = 1/(1 - 4\pi\alpha_{zz}^{2D}/V)$ or $4\pi\alpha_{zz}^{2D}/V = (\epsilon_{zz} - 1)/\epsilon_{zz}$, which leads to

$$\frac{\partial \alpha_{zz}^{3D}}{\partial \mathcal{R}_x^A} = \epsilon_{zz} \frac{\partial \alpha_{zz}^{2D}}{\partial \mathcal{R}_x^A} + \frac{\epsilon_{zz} - 1}{\epsilon_{zz}} \frac{\partial \alpha_{zz}^{3D}}{\partial \mathcal{R}_x^A} \tag{A4}$$

so that, finally,

$$\frac{d\alpha_{zz}^{3D}}{d\mathcal{R}_x^A} = \epsilon_{zz}^2 \frac{\partial \alpha_{zz}^{2D}}{\partial \mathcal{R}_x^A}. \tag{A5}$$

Let us turn now to the case of the off-diagonal component $\alpha_{xz}^{3D} = \alpha_{zx}^{3D} = (d\mu_x/d\mathcal{E}_z + d\mu_z/d\mathcal{E}_x)/2$ (with the equality $d\mu_x/d\mathcal{E}_z = d\mu_z/d\mathcal{E}_x$), and its derivative with respect to $\mathcal{R}_z^A$: $d\alpha_{xz}^{3D}/d\mathcal{R}_z^A$. As we have seen above, the calculation of the polarizability of the bulk and slab is different if either, or both components is along z since the field in that direction is not the same ($\mathcal{E}_{0z} = \epsilon_{zz}\mathcal{E}_z$) nor is the dipole moment operator, which is Ω_z for the bulk, but z for the slab. Then, we have

$$\begin{aligned} \alpha_{zx}^{3D} &= \frac{d\mu_z}{d\mathcal{E}_x} = \frac{d\mu_z}{d\mathcal{E}_{0x}} \frac{d\mathcal{E}_{0x}}{d\mathcal{E}_x} = \alpha_{zx}^{2D} \\ = \alpha_{xz}^{3D} &= \frac{d\mu_x}{d\mathcal{E}_z} = \frac{d\mu_x}{d\mathcal{E}_{0z}} \frac{d\mathcal{E}_{0z}}{d\mathcal{E}_z} = \epsilon_{zz}\alpha_{xz}^{2D}. \end{aligned} \tag{A6}$$

Following the previous demonstration for the diagonal component, the derivative of α_{xz}^{3D} with respect to $\mathcal{R}_z^A$ leads to

$$\frac{d\alpha_{xz}^{3D}}{d\mathcal{R}_z^A} = \frac{\partial \alpha_{xz}^{3D}}{\partial \mathcal{R}_z^A} + \frac{\partial \alpha_{xz}^{3D}}{\partial \mathcal{E}_z} \frac{\partial \mathcal{E}_z}{\partial \mathcal{R}_z^A}. \tag{A7}$$

In this case, the second term on the rhs is not null since the hyperpolarizability component $\beta_{xzz}^{3D} = \partial\alpha_{xz}^{3D}/\partial\mathcal{E}_z$ is not equal to zero. The partial derivative $\partial\mathcal{E}_z/\partial\mathcal{R}_z^A$ is related to the derivative of the polarization vector $4\pi\mathcal{P}_z = -4\pi\mu_z^{3D}/V = \mathcal{E}_z - \mathcal{E}_{0z}$ with respect to the atomic displacement $\mathcal{R}_z^A$ as follows:

$$\frac{\partial \mathcal{E}_z}{\partial \mathcal{R}_z^A} = -\frac{4\pi}{V} \frac{\partial \mu_z^{3D}}{\partial \mathcal{R}_z^A}, \tag{A8}$$

which corresponds to the effective charge of the slab $Z_{zz}^{*2D} = -(\partial\mu_z^{2D}/\partial\mathcal{R}_z^A)$ since, for zero field, $\mu_{zz}^{3D} = \mu_{zz}^{2D}$. Then, using $\partial\mathcal{E}_z/\partial\mathcal{R}_z^A$ by $4\pi Z_{zzA}^{*2D}/V$ in Eq. (A7), and the definition of the second nonlinear electric susceptibility component (see also Eq. (75) in Ref. 15)

$$\chi_{xzz}^{(2)} = \frac{2\pi}{V}\beta_{xzz}^{3D} = \frac{2\pi}{V}\frac{\partial \alpha_{xz}^{3D}}{\partial \mathcal{E}_z}, \tag{A9}$$

Eq. (A7) becomes

$$\frac{d\alpha_{xz}^{3D}}{d\mathcal{R}_z^A} = \frac{\partial \alpha_{xz}^{3D}}{\partial \mathcal{R}_z^A} + 2\chi_{xzz}^{(2)} Z_{zzA}^{*2D}. \tag{A10}$$

Since $\partial\epsilon_{zz}/\partial\mathcal{R}_z^A = 0$ in cubic LiF, we may utilize Eq. (A6) to obtain the final result

$$\frac{d\alpha_{xz}^{3D}}{d\mathcal{R}_z^A} = \epsilon_{zz} \frac{\partial \alpha_{xz}^{2D}}{\partial \mathcal{R}_z^A} + 2\chi_{xzz}^{(2)} Z_{zzA}^{*2D}. \tag{A11}$$

Note that the a.u. system has been used in this work, in which case $4\pi\epsilon_0$ (where ϵ_0 is the the dielectric permittivity of the vacuum) is equal to 1.

[1] L. Maschio, B. Kirtman, M. Rérat, R. Orlando, and R. Dovesi, J. Chem. Phys. **139**, 164101 (2013).
[2] G. Placzek, *Handbuch der Radiologie* (Akademische Verlagsgeselschft, Leipzig, 1934), Vol. 6, p. 208.
[3] R. Dovesi, V. R. Saunders, C. Roetti, R. Orlando, C. M. Zicovich-Wilson, F. Pascale, K. Doll, N. M. Harrison, B. Civalleri, I. J. Bush *et al.*, *CRYSTAL09 User's Manual* (Università di Torino, Torino, 2009).
[4] R. Dovesi, R. Orlando, B. Civalleri, C. Roetti, V. Saunders, and C. Zicovich-Wilson, Z. Kristallogr. **220**, 571 (2005).
[5] P. Umari, A. Pasquarello, and A. D. Corso, Phys. Rev. B **63**, 094305 (2001).
[6] S. Baroni, S. de Gironcoli, A. dal Corso, and P. Giannozzi, Rev. Mod. Phys. **73**, 515 (2001).
[7] G. Deinzer and D. Strauch, Phys. Rev. B **66**, 100301(R) (2002).
[8] M. Lazzeri and F. Mauri, Phys. Rev. Lett. **90**, 036401 (2003).
[9] M. Veithen, X. Gonze, and P. Ghosez, Phys. Rev. B **71**, 125107 (2005).
[10] K. Miwa, Phys. Rev. B **84**, 094304 (2011).
[11] S. A. Prosandeev, U. Waghmare, I. Levin, and J. Maslar, Phys. Rev. B **71**, 214307 (2005).
[12] R. Caracas and E. J. Banigan, Phys. Earth Planet. Inter. **174**, 113 (2009).
[13] D. A. McKeown, M. I. Bell, and R. Caracas, Am. Mineral. **95**, 980 (2010).
[14] See http://www.wurm.info for a database of Raman spectra of minerals simulated with plane wave basis and LDA functional.
[15] M. Ferrero, M. Rérat, B. Kirtman, and R. Dovesi, J. Chem. Phys. **129**, 244110 (2008).
[16] L. Maschio, B. Kirtman, R. Orlando, and M. Rérat, J. Chem. Phys. **137**, 204113 (2012).
[17] Y. Saito and P. Verma, J. Phys. Chem. Lett. **3**, 1295 (2012).
[18] S. T. Meek, J. A. Greathouse, and M. D. Allendorf, Adv. Mater. **23**, 249 (2011).
[19] J. H. Cavka, S. Jakobsen, U. Olsbye, N. Guillou, C. Lamberti, S. Bordiga, and K. P. Lillerud, J. Am. Chem. Soc. **130**, 13850 (2008).
[20] M. Ferrero, M. Rérat, R. Orlando, and R. Dovesi, J. Comput. Chem. **29**, 1450 (2008).
[21] M. Ferrero, M. Rérat, R. Orlando, and R. Dovesi, J. Chem. Phys. **128**, 014110 (2008).
[22] K. Doll, N. M. Harrison, and V. R. Saunders, Int. J. Quantum Chem. **82**, 1 (2001).
[23] The adopted thresholds are 10^{-12} for the SCF convergence on energy, 10^{-6} for the convergence on the polarizability α in the CPHF iterative procedure; a two-point formula has been used numerical second-order derivatives with respect to atomic positions, with a step size = 0.001 Å.
[24] R. Dovesi, C. Pisani, C. Roetti, and V. R. Saunders, Phys. Rev. B **28**, 5781 (1983).
[25] M. Causà, R. Dovesi, R. Orlando, C. Pisani, and V. R. Saunders, J. Phys. Chem. **92**, 909 (1988).
[26] Geometry was optimized for the chosen basis set with the lattice parameters fixed at $a = 4.916$ Å and $c = 5.405$ Å. A 8-411d11 basis was adopted on oxygen,[28] and 86-311d on Si.[32]
[27] V. Solozhenko, G. Will, and F. Elf, Solid State Commun. **96**, 1 (1995).
[28] L. Valenzano, Y. Noel, R. Orlando, C. M. Zicovich-Wilson, M. Ferrero, and R. Dovesi, Theor. Chem. Acc. **117**, 991 (2007).
[29] M. Cardona and G. Güntherodt, *Light Scattering in Solids II* (Springer-Verlag, Berlin, 1982).
[30] W. D. Johnston, Phys. Rev. B **1**, 3494 (1970).
[31] See www.crystal.unito.it for more details and information about the CRYSTAL code.
[32] Y. Noel, M. Catti, P. D'Arco, and R. Dovesi, Phys. Chem. Miner. **33**, 383 (2006).
[33] L. Valenzano, F. Torres, K. Doll, F. Pascale, C. Zicovich-Wilson, and R. Dovesi, Z. Phys. Chem. **220**, 893 (2006).
[34] M. F. Peintinger, D. V. Oliveira, and T. Bredow, J. Comput. Chem. **34**(6), 451 (2013).
[35] C. M. Zicovich-Wilson, F. Pascale, C. Roetti, R. Orlando, V. R. Saunders, and R. Dovesi, J. Comput. Chem. **25**, 1873 (2004).
[36] C. Carteret, L. Maschio, V. Lacivita, and R. Dovesi, "The Raman spectrum of α-quartz: A combined experimental and quantum mechanical investigation" (unpublished).

[37]R. L. McCreery, in *Handbook of Vibrational Spectroscopy*, edited by J. Chalmers and P. Griffiths (John Wiley & Sons, Ltd., Chichester, 2002), pp. 920–932.
[38]M. D. Halls and H. B. Schlegel, J. Chem. Phys. **111**, 8819 (1999).
[39]C. A. Jiménez-Hoyos, B. G. Janesko, and G. E. Scuseria, Phys. Chem. Chem. Phys. **10**, 6621 (2008).
[40]A number of high quality Raman spectra can be found, for α-quartz powder, in literature or on the web. The one reported is one of the cleanest we have found, and has been downloaded from the Handbook of Minerals Raman Spectra database of Lyon ENS (http://www.ens-lyon.fr/LST/Raman/).
[41]S. Chavan, J. G. Vitillo, M. J. Uddin, F. Bonino, C. Lamberti, E. Groppo, K.-P. Lillerud, and S. Bordiga, Chem. Mater. **22**, 4602 (2010).
[42]L. Valenzano, B. Civalleri, S. Chavan, S. Bordiga, M. H. Nilsen, S. Jakobsen, K. P. Lillerud, and C. Lamberti, Chem. Mater. **23**, 1700 (2011).
[43]Hamiltonian is B3LYP. All electron basis sets were used for Zr, O, C, and H atoms; they consist of (8*s*)-(7631*sp*)-(621*d*), (8*s*)-(411*sp*)-(1*d*), (6*s*)-(31*sp*)-(1*d*), and (31*s*)-(1*p*), respectively. All parameters except shrinking factor (here raised to 3 from the original value of 2) are identical as in the CRYSTAL input reported in the supplementary material of Ref. 42 (hydroxilated-UiO-66).
[44]See http://www.crystal.unito.it/vibs/uio66_hydro/ for the visualization of UiO-66 vibrational modes.
[45]M. Kandiah, M. H. Nilsen, S. Usseglio, S. Jakobsen, U. Olsbye, M. Tilset, C. Larabi, E. A. Quadrelli, F. Bonino, and K. P. Lillerud, Chem. Mater. **22**, 6632 (2010).